Article citation info:
Taouil M, El Ougli A, Tidhaf B. Actuator fault estimation in wind turbine using a modified sliding mode observer based on linear matrix inequality approach. Diagnostyka. 2024;25(2):2024211. https://doi.org/10.29354/diag/187887.

DIAGNOSTYKA, 2024, Vol. 25, No. 2

e-ISSN 2449-5220
DOI: 10.29354/diag/187887

ACTUATOR FAULT ESTIMATION IN WIND TURBINE USING A MODIFIED SLIDING MODE OBSERVER BASED ON LINEAR MATRIX INEQUALITY APPROACH

Mohammed TAOUIL [1, *], Abdelghani EL OUGLI [2], Belkassem TIDHAF [3]

[1] Electronics and Systems Laboratory - LES, Faculty of Sciences Oujda, Embedded Systems, Renewable Energy and Artificial Intelligence Team, ENSA, Oujda, Morocco.
[2] Computer Science, Signal, Automation and Cognitivism Laboratory (LISAC), Faculty of Science Sidi Mohamed Ben Abdellah University, Fez, Morocco
[3] Embedded Systems, Renewable Energy and Artificial Intelligence Team, National School of Applied Sciences, Mohammed First University, Oujda, Morocco
[*] Corresponding author, e-mail: t123med@hotmail.fr

Abstract

This paper presents a fault detection and isolation (FDI) method applied to a wind turbine system. The approach utilizes a nonlinear sliding mode observer (SMO) to effectively reconstruct faults in both the hydraulic pitch actuator and generator torque actuator of the wind turbine. A Linear Matrix Inequality (LMI) optimization approach is employed for the design. The blade pitch angle and generator torque in the wind turbine have significantly different orders of magnitudes, rendering them vulnerable to faults of different magnitudes. This discrepancy poses a challenge for the simultaneous reconstruction of faults. To resolve this challenge, a modification is made to the observer. To examine the effectiveness of the modified SMO, two fault scenarios were considered for the hydraulic pitch actuator and generator torque actuator. In the first case, faults are introduced separately, while in the second case, faults occur simultaneously. Simulation results demonstrate accurate detection, isolation, and reconstruction of these faults, whether in the case of separate or simultaneous fault occurrences.

Keywords: actuator fault reconstruction, faults separately, faults simultaneously, Modified sliding mode observer

List of Symbols/Acronyms

DIS – discontinuous injection switching
FDI – Fault Detection and Isolation;
FTC – fault tolerant control;
SMO–Sliding Mode Observer;
WTBM–wind turbine benchmark model;
B_{dt}– drive train torsion damping coefficient [N.m.s.rad^{-1}];
B_r–viscous friction of the low-speed shaft [N.m.s.rad^{-1}];
B_g–generator viscous friction [N.m.s.rad^{-1}];
$C_q(\beta, \lambda)$–torque coefficient;
J_r– inertial moment of the low-speed shaft [kg.m^{-2}];
J_g–generator moment of inertia [kg.m^{-2}];
K_{dt}– torsional stiffness of the drive system [N.m.rad^{-1}];
N_g–gear ratio;
β– pitch angle [deg];
β_{re}–reference pitch angle [deg];
τ_g–generator torque [N.m];
τ_{gre} –reference generator torque [N.m];
τ_r–rotor torque [N.m];
θ– Drive train torsion angle [rad];
λ –tip speed ratio;
ξ – damping coefficient;
$1/\alpha_{gc}$– time constant [s];
ω_g–generator angular speed [$rad.s^{-1}$];
ω_r–rotor angular speed [$rad.s^{-1}$];
v_w–wind speed [$m.s^{-1}$];
w_n – natural pulsation [$rad.s^{-1}$].

1. INTRODUCTION

In 2022, global wind energy capacity increased by 78 GW, reaching a total of 906 GW. 2023 is projected to be the first year to exceed 100 GW in new capacity, with a 15% year-on-year growth rate forecasted. Over the next five years (2023-2027), 680 GW of new capacity is expected, averaging 136 GW per year. By 2030, an additional 143 GW is anticipated, 13% higher than previous estimates, for a total of 1221 GW added from 2023 to 2030. These figures highlight the substantial growth and potential of wind energy on a global scale [1].

The rapid growth of wind turbines necessitates greater efficiency but faces complexities and susceptibility to faults due to environmental factors

Received 2023-09-29; Accepted 2024-04-23; Available online 2024-04-23

and manufacturing defects [2]. Their remote, isolated locations make maintenance challenging, potentially leading to breakdowns that can influence electricity production. Consequently, there is a growing interest in employing FDI methods, especially for critical components like pitch and drive train systems, to address these challenges in wind turbine systems [3-4].

Specifically for fault detection purposes, a validated WTBM was developed by Odgaard et al. [5]. Building upon this model, numerous approaches have been introduced in recent years in the fields of model-based fault diagnosis (FD) and FTC for WTBM [6-7]. FDI in wind turbines aims to issue timely warnings for abnormal situations and locate their source. FDI methods fall into two categories: data-driven and model-based. Data-driven methods, such as those employing fuzzy systems and neural networks, can be effective but may experience delays due to the requirement for data collection [8]. Model-based FDI techniques for wind turbines employ computational representations to mimic how these systems function in both standard and malfunctioning states. These strategies hinge on matching the outcomes from these computational models to actual sensor readings to pinpoint and separate out faults. A commonly used approach in this field is the observer-based technique. This approach entails creating 'observers,' alternatively referred to as estimators or filters, which make use of sensor data to gauge the wind turbine's internal conditions. When these computed conditions are set against real-world measurements, any discrepancies can be identified as faults, which can then be attributed to specific issues. Various specialized observer-based FDI methodologies have been designed, particularly for wind turbine systems [9-10]. Cho et al. [11] utilize a Kalman filter and inference algorithms to detect, isolate, and control faults in the blade pitch systems of floating wind turbines. In [12], an adaptive observer-based scheme using the Fast Adaptive Fault Estimation (FAFE) algorithm swiftly detects sensor and actuator faults, enabling controllers to stabilize and compensate for these faults more effectively than baseline methods. Most FDI methods for wind turbines rely on generating residuals, which compare actual system outputs to observer predictions. These approaches, however, are susceptible to false alarms due to environmental disturbances and model uncertainties. To be effective, FDI schemes must therefore be robust, minimizing sensitivity to these uncertainties while maintaining alertness to actual faults [13]. In [14], a robust fault estimation method is presented. The proposed observer-based scheme adeptly identifies sensor and actuator faults within wind turbines, employing a two-step approach to distinguish unknown inputs from actual faults. Shi and Patton [15] crafted a unique Active FTC system for large, non-linear rotor wind turbines using observer-based methods, leveraging Linear Matrix Inequality (LMI) within a Linear Parameter Varying (LPV) framework. The scheme focuses on hiding sensor faults and compensating for actuator faults.

Sliding Mode Observers are extensively employed for robust fault detection, isolation, and fault-tolerant control in wind turbines due to their inherent robustness [16-18]. While these techniques are generally effective, they do have a weak point: they often rely on predefined thresholds based on known fault behaviour, which presents a major limitation for this technique. In [19], a sliding mode observer is employed with a suggested modification for the nonlinear switching term to reconstruct sensor faults in wind turbines. The accuracy is satisfactory; however, actuator faults remain unaddressed.

This paper employs a 4.8 MW wind turbine benchmark model to analyze faults across different components. It introduces an FDI scheme capable of not only detecting but also accurately reconstructing faults, making it suitable for FTC schemes requiring knowledge of fault magnitudes. Additionally, a modified fault estimation approach based on the SMO is presented. A Matrix Inequality (LMI) optimization approach is utilized for the design of the SMO aimed at proficiently detecting, isolating, and estimating actuator faults in the WTBM impacting blade pitch angle actuator and generator torque actuator. This modification addresses the DSI of the observer for precise reconstruction, notably in simultaneous faults scenarios. The simulations are implemented within the MATLAB/Simulink environment. The structure of this paper is outlined as follows: Section 2 provides a concise overview of the Wind Turbine Benchmark Model (WTBM); Section 3 elaborates on the fault estimation approach, formulation of the actuator faults, suggested enhancements to the SMO, and numerical specifications for its parameters; Section 4 explores different fault scenarios and expounds on the simulation results; finally, Section 5 summarizes the conclusions derived from the study.

2. MODEL OF WIND TURBINE

This study is based on a model of a three-bladed horizontal axis wind turbine, similar to the one studied in [5]. The system layout comprises interconnected subsystems: the Blade & Pitch System, Drive Train, Converter, and Generator, as illustrated in Figure 1. Aerodynamic behaviour, influenced by blade pitch angles, rotor characteristics, and wind speed, powers the wind energy system by transferring aerodynamic torque from the drive train to the generator, where it is converted into electrical energy. A controller, detailed in [5], adjusts blade pitch angles and generator torque to meet operational requirements. The ensuing description elucidates the mathematical representation for each constituent of the WTBM depicted in Figure 1.

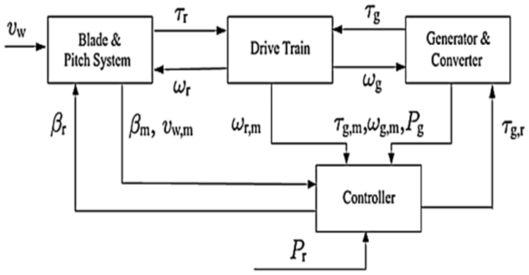

Fig. 1. Synopsis of the WTBM [5]

2.1. Subsystem: Blade - Pitch

This subsystem combines the aerodynamic model, blades, and pitch system, with the aerodynamic torque being determined by:

$$\tau_r = \frac{\rho \pi R^3 C_q\big(\beta(t), \lambda(t)\big) v_w^2}{2} \qquad (1)$$

The pitching system encompasses three actuators, each embedded with an internal controller. These actuators, denoted as actuator i (where i can take values 1, 2, or 3), are responsible for adjusting the pitch angle β_i of the blades. The following second-order transfer function represents this subsystem:

$$\frac{\beta_i(s)}{\beta_{re,i}} = \frac{\omega_{ni}^2}{s^2 + 2.\xi_i.\omega_{ni}.s + \omega_{ni}^2} \qquad (2)$$

In the absence of faults, all values of β_i, ω_{ni}, and ξ_i are equal. However, if faults occur, these values can vary from one another. In the subsequent analysis, only a single pitch actuator is taken into account.

2.2. Subsystem: Drive train

Utilizing a simplified two-mass model, the representation of the drive train system is achieved. This allows the drive train model to be depicted as:

$$\begin{cases} J_g.\dot{\omega}_g = -\left(\frac{\eta_{dt}B_{dt}}{N_g^2} + B_g\right)\omega_g + \frac{\eta_{dt}B_{dt}}{N_g}\omega_r + \frac{\eta_{dt}K_{dt}}{N_g}\theta - \tau_g & (3) \\ J_r\dot{\omega}_r = \frac{B_{dt}}{N_g}\omega_g - (B_{dt} + B_r)\omega_r - K_{dt}\theta + \tau_r & (4) \\ \dot{\theta} = \omega_r - \frac{1}{N_g}\omega_g & (5) \end{cases}$$

2.3. Subsystem: Generator-Converter

In this block, mechanical energy is transformed into electrical energy. This subsystem is modeled by first-order transfer functions:

$$\frac{\tau_g}{\tau_{gre}} = \frac{1}{1 + {}^{1}/_{\alpha_{gc}}\, s} \qquad (6)$$

The output power generated is expressed as:

$$P_g = \eta_g.\tau_g.\omega_g \qquad (7)$$

η_g refers to the efficiency of the generator.

By combining and integrating the aforementioned subsystems, the wind system is represented in the state space using the following model:

$$\begin{cases} \dot{x}(t) = A\,x(t) + B\,u(t), & (8) \\ y(t) = C\,x(t). & (9) \end{cases}$$

The state vector, denoted as $x = [\omega_g \quad \omega_r \quad \theta \quad \dot{\beta} \quad \beta \quad \tau_g]^T$, represents the system's state. The control input vector, $u = [\tau_{gre} \quad \tau_r \quad \beta_{re}]^T$, represents the inputs that control the system.

$$B = \begin{bmatrix} 0 & 0 & 0 \\ 0 & \frac{1}{J_g} & 0 \\ 0 & 0 & 0 \\ 0 & 0 & \omega_n^2 \\ 0 & 0 & 0 \\ \alpha_{gc} & 0 & 0 \end{bmatrix}, C = \begin{bmatrix} 1 & 0 & 0 & 0 & 0 & 0 \\ 0 & 1 & 0 & 0 & 0 & 0 \\ 0 & 0 & 0 & 1 & 0 & 0 \\ 0 & 0 & 0 & 0 & 1 & 0 \\ 0 & 0 & 0 & 0 & 0 & 1 \end{bmatrix},$$

$$A = \begin{bmatrix} a_{11} & \frac{\eta_{dt}B_{dt}}{N_gJ_g} & \frac{\eta_{dt}K_{dt}}{N_gJ_g} & 0 & 0 & -\frac{1}{J_g} \\ \frac{B_{dt}}{N_gJ_r} & -\frac{B_{dt}+B_r}{J_r} & -\frac{K_{dt}}{J_r} & 0 & 0 & 0 \\ -\frac{1}{N_g} & 1 & 0 & 0 & 0 & 0 \\ 0 & 0 & 0 & -2\xi\omega_n & -\omega_n^2 & 0 \\ 0 & 0 & 0 & 1 & 0 & 0 \\ 0 & 0 & 0 & 0 & 0 & -\alpha_{gc} \end{bmatrix},$$

$$a_{11} = -\frac{\frac{\eta_{dt}B_{dt}}{N_g^2} + B_g}{J_g}.$$

3. SCHEME FOR ESTIMATING FAULTS

3.1. Design of sliding mode observer

The system of equations (10)-(11) describes the wind system that can be affected by an actuator fault:

$$\begin{cases} \dot{x}(t) = A\,x(t) + B\,u(t) + D\,f_{ac}(t, x, u) & (10) \\ y(t) = C\,x(t) & (11) \end{cases}$$

Let $A \in \mathbb{R}^{n\times n}$, $C \in \mathbb{R}^{p\times n}$, $B \in \mathbb{R}^{n\times m}$, and $D \in \mathbb{R}^{n\times q}$, where $p \geq q$. Assuming that the matrices C and D are full rank, and that the function f_{ac} represents a bounded actuator fault satisfies:

$$\|f_{ac}\| \leq \lambda\|u\| + \sigma \qquad (12)$$

Where: λ is a known positive scalar and σ is a known positive function.

Aiming to craft an observer, its primary function is to estimate the system's state vector $\hat{x}$ and its output vector $\hat{y}$ from the signals u(t) and y(t). With the system state assumed to be unknown, our ultimate objective is to ensure that the output error $\varepsilon_y(t) = \hat{y}(t) - y(t)$ promptly converges to zero, irrespective of any faults. Edwards and Spurgeon [19] proposed an observer:

$$\dot{\hat{x}} = A\hat{x} + Bu - G_l\varepsilon_y + G_n\vartheta. \qquad (13)$$

ϑ the DIS, is given by

$$\vartheta = \begin{cases} -\kappa \left\|P_0\, \widetilde{D}_2\right\| \frac{\varepsilon_y}{\|\varepsilon_y\|}, & if\ \varepsilon_y \neq 0 \\ 0 & otherwise \end{cases} \qquad (14)$$

The function κ satisfies:

$$\kappa > \|f_{ac}\| \qquad (15)$$

If the state estimation error $\varepsilon = \hat{x} - x$, then

$$\dot{\varepsilon} = A_0\varepsilon + G_n\vartheta - D\,f_{ac} \qquad (16)$$

Where $A_0 = A - G_lC$.

The matrices P_0, $\widetilde{D}_2$, G_l, and G_n are to be determined.

3.2. Observer Modifications

The wind turbine outputs, specifically ω_r, ω_g, β and τ_g differ substantially in magnitude, with values around $1 rad/s, 10^2 rad/s$, $1 deg$, and $10^4 N.m$ respectively. Equations (39) and (40) allow for the reconstruction of actuator faults, emphasizing the dependence on the scalar gain, nearly matching the fault's peak magnitude. While the gain, κ, must be tailored for each output, the conventional SMO uses a static κ, hindering accurate fault detection for all outputs. Continually adjusting κ, especially with concurrent faults across various outputs, is unfeasible. As a solution, κ is substituted with $\kappa' = \alpha\|P_0\varepsilon_y\|$, and ε_y is replaced by $P_0\varepsilon_y$, leading to a revised switching term:

$$\vartheta = -\kappa'.\|P_0\,\widetilde{D}_2\|\frac{P_0\varepsilon_y}{\|P_0\varepsilon_y\|} \tag{17}$$

This modification allows for a more adaptive approach, where $\alpha\|P_0\varepsilon_y\|$ is utilized to adjust κ based on the specific output being considered. The scalar α is chosen such that

$$\alpha > \lambda\|u\| + \sigma \tag{18}$$

3.3. A framework for SMO desing

The integration of Linear Matrix Inequalities (LMI) in fault reconstruction holds significant importance. LMIs provide a powerful mathematical framework, enabling precise modelling of dynamic relationships and establishing essential stability and performance conditions to ensure the validity of estimations. By optimizing observer gains through LMIs, the quality of fault reconstruction improves, and uncertainties inherent in operational variations are effectively managed, ensuring the robustness of estimations. This capability facilitates practical implementation, contributing to reliable and efficient fault reconstruction. Furthermore, Edwards et al. [19] propose a systematic method for computing gains G_l and G_n, but this method does not fully exploit all available degrees of freedom. The following section explores the design of matrices G_l, G_n, and P_0 based on an LMI approach, aiming to maximize the utilization of all available degrees of freedom.

It is shown in [20] that the observer of the form (13) exists if and only if:

1. rank(CD)=q,
2. invariant zeros of (A,D,C) are stable

Furthermore, if these two conditions are satisfied, then there exist a change of coordinates T_0 such that the previous system can be written as:

$$\begin{cases}\underline{\dot{x}}(t) = \underline{A}\,\underline{x}(t) + \underline{B}\,u(t) + \underline{D}\,f_{ac}(t,x,u) & (19)\\ y(t) = \underline{C}\,\underline{x}(t) & (20)\end{cases}$$

where $\underline{x} = T_0 x$. The triple $(\underline{A}, \underline{D}, \underline{C})$ has the following structure:

$$\underline{A} = \begin{bmatrix} A_{11} & A_{12} \\ A_{21} & A_{22}\end{bmatrix},\ \underline{D} = \begin{bmatrix} 0 \\ D_2\end{bmatrix},\ \underline{C} = [0 \quad T] \tag{21}$$

Where $T \in \mathbb{R}^{p\times p}$ is orthogonal.

The change of coordinates applied to relation (14) allows for obtaining

$$\underline{\dot{\hat{x}}} = \underline{A}\underline{\hat{x}} + \underline{B}u - \underline{G_l}\varepsilon_y + \underline{G_n}\vartheta \tag{22}$$

And define $\underline{A_0} = \underline{A} - \underline{G_l}\underline{C}$ .The gain matrix $\underline{G_l}$ is to be determined but $\underline{G_n}$ is given by:

$$\underline{G_n} = \begin{bmatrix} -\underline{L}T^T \\ T^T \end{bmatrix} \tag{23}$$

Where $\underline{L} \in \mathbb{R}^{(n-p)\times p}$ and has the structure $\underline{L} = [L \quad 0]$ with $L \in \mathbb{R}^{(n-p)\times(n-q)}$ to be determined.

Proposition: If a positive definite Lyapunov matrix $\underline{P}$ exists such that $\underline{P}\underline{A_0} + \underline{A_0^T}\underline{P} < 0$, with the specified structure:

$$\underline{P} = \begin{bmatrix} \underline{P_1} & \underline{P_1}\underline{L} \\ \underline{L^T}\underline{P_1} & \underline{P_0} + \underline{L^T}\underline{P_1}\underline{L}\end{bmatrix} > 0 \tag{24}$$

Where $\underline{P_1} \in \mathbb{R}^{(n-p)\times(n-p)}$ and $\underline{P_0} \in \mathbb{R}^{p\times p}$, then the error in equation (16) is quadratically stable.

Proof: Let's consider the quadratic form

$$\nu = \underline{\varepsilon}^T \underline{P}\,\underline{\varepsilon} \tag{25}$$

as a candidate Lyapunov function where $\underline{\varepsilon} = T_0\varepsilon$.

$$\begin{aligned}\dot{\nu} = \underline{\varepsilon}^T\left(\underline{A_0^T}\underline{P} + \underline{P}\underline{A_0}\right)\underline{\varepsilon} + 2\underline{\varepsilon}^T\underline{P}\underline{G}_n\vartheta \\ - 2\varepsilon^T\underline{P}\underline{D}f_{ac}\end{aligned} \tag{26}$$

From (21),(23), and (24)

$$\underline{P}\underline{G}_n = \begin{bmatrix} 0 \\ \underline{P_0}T^T\end{bmatrix} = \underline{C}^T P_0 \tag{27}$$

Where $P_0 = T\underline{P}_0 T^T$

Employing the specific structure of $\underline{L}$ and $\underline{D}$, $\underline{L}D_2 = 0$ as a result

$$\underline{P}\underline{D} = \begin{bmatrix} 0 \\ \underline{P_0}D_2\end{bmatrix} = \underline{C}^T P_0\widetilde{D}_2 \tag{28}$$

Where $\widetilde{D}_2 = TD_2$ which implies $\|\widetilde{D}_2\| = \|D_2\|$

By incorporating the modification of ϑ into equation (17), equation (26) becomes

$$\dot{\nu} = \underline{\varepsilon}^T\left(\underline{A_0^T}\underline{P} + \underline{P}\underline{A_0}\right)\underline{\varepsilon} + 2\varepsilon_y^T P_0\vartheta - 2\varepsilon_y^T P_0\widetilde{D}_2 f_{ac}$$

$$\begin{aligned}\leq \underline{\varepsilon}^T\left(\underline{A}_0^T\underline{P} + \underline{P}\underline{A}_0\right)\underline{\varepsilon} - 2\alpha\|P_0\varepsilon_y\|^2.\|P_0\,\widetilde{D}_2\| \\ - 2\varepsilon_y^T P_0\widetilde{D}_2 f_{ac}\end{aligned}$$

Utilizing equations (12) and (18)

$$\begin{aligned}\dot{\nu} \leq \underline{\varepsilon}^T\left(\underline{A_0^T}\underline{P} + \underline{P}\underline{A_0}\right)\underline{\varepsilon} - 2[\lambda\|u\| + \sigma]\|P_0\varepsilon_y\|^2\,\|P_0\,\widetilde{D}_2\| \\ + 2\|\widetilde{D}_2\|\,[\lambda\|u\| + \sigma]\,\|P_0\varepsilon_y\|\end{aligned}$$

$$\dot{\nu} \leq \underline{\underline{\varepsilon}}^T\left(\underline{A_0^T}\underline{P} + \underline{P}\underline{A_0}\right)\underline{\varepsilon} - 2.J$$

Where

$J = [\lambda\|u\| + \sigma].\left[\|P_0\, \tilde{D}_2\|\|P_0\varepsilon_y\| + \|\tilde{D}_2\|\right].\|P_0\varepsilon_y\| \geq 0$

Since $\underline{P}\underline{A}_0 + \underline{A}_0^T\underline{P} < 0$ it follows that $\dot{v} < 0$ for all $\underline{\varepsilon} \neq 0$ and quadratic stability is proved.

3.4. Procedural Synthesis of Matrices $\underline{P}$ and $\underline{\boldsymbol{G}}_l$

a method for observer design through the use of LMIs was put forth by Alwi et al. [20]. This design approach can be succinctly described as:
Matrices $\underline{P}$ and $\underline{G}_l$ are selected to ensure satisfaction of the subsequent matrix inequality

$$\underline{P}\underline{A}_0 + \underline{A}_0^T\underline{P} < -\underline{P}U_w\underline{P} - \underline{P}\underline{\boldsymbol{G}}_l V_w \underline{G}_l^T\underline{P} \qquad (29)$$

$U_w \in \mathbb{R}^{n\times n}$ and $V_w \in \mathbb{R}^{p\times p}$ are presumed to be symmetric positive definite design weighting matrices, assumed known, with $\underline{P}$ structured according to equation (24). By introducing the matrix $\underline{Y} = \underline{P}\underline{\boldsymbol{G}}_l$ and substituting the expression for $\underline{A}_0$, inequality (29) takes the following form

$$\underline{P}\,\underline{A} + \underline{A}^T\underline{P} + \left(\underline{Y}^T - V_w^{-1}\underline{C}\right)V_w\left(\underline{Y}^T - V_w^{-1}\underline{C}\right) - \underline{C}^T V_w^{-1}\underline{C} + \underline{P}\,U_w\underline{P} < 0 \qquad (30)$$

The choice $\underline{Y}^T = V_w^{-1}\underline{C}$ implies

$$\underline{P}\,\underline{A} + \underline{A}^T\underline{P} - V_w^{-1}\underline{C} + \underline{P}\,U_w\underline{P} < 0 \qquad (31)$$

And $\underline{\boldsymbol{G}}_l = \underline{P}^{-1}C^T V_w^{-1}$

The problem under consideration involves minimizing $\mathrm{trace}(P^{-1})$ while satisfying inequality (31). The matrix inequality in (31), by using the Schur complement, is equivalent to

$$\begin{bmatrix} P\underline{A} + \underline{A}^T P - \underline{C}^T V_w{}^{-1}\underline{C} & P \\ P & -U_w{}^{-1} \end{bmatrix} < 0 \qquad (32)$$

$$\begin{bmatrix} -P & I \\ I & -X \end{bmatrix} < 0 \qquad (33)$$

Where $X, P \in \mathbb{R}^{n\times n}$ are s.p.d matrix variables. Standard LMI software can be employed to resolve simultaneously LMIs (32) and (33), This enables the synthesis of P, which has the structure:

$$\underline{P} = \begin{bmatrix} P_{11} & P_{12} \\ P_{12}^T & P_{22} \end{bmatrix} > 0 \qquad (34)$$

Where $P_{11} \in \mathbb{R}^{(n-p)\times(n-p)}$, $P_{22} \in \mathbb{R}^{p\times p}$ and $P_{12} = [P_{121} \quad 0]$ with $P_{121} \in \mathbb{R}^{(n-p)\times(p-q)}$, $P_{22} \in \mathbb{R}^{p\times p}$, define:

$$L = [P_{11}^{-1}P_{121} \quad 0] \qquad (35)$$

The matrix P_0, which appears in (37), is given by:

$$P_0 = T(P_{22} - P_{12}^T P_{11}^{-1} P_{12})T^T \qquad (36)$$

To exploit the gains Gl and Gn in relation (13), it is necessary to multiply them by the inverse of a transformation matrix T_0 [19], as in equations (37)

$$G_l = T_0^{-1}P^{-1}\underline{C}^T V_w{}^{-1} \text{ and } G_n = T_0^{-1}\begin{bmatrix} -LT^T \\ T^T \end{bmatrix} P_0^{-1} \qquad (37)$$

Subsequently, a coordinate transformation is implemented:
$T_* = \begin{bmatrix} I_{n-p} & L \\ 0 & T \end{bmatrix}$, transforms the triplet (A, D, C) to:

$$\tilde{A} = \begin{bmatrix} \tilde{A}_{11} & \tilde{A}_{12} \\ \tilde{A}_{21} & \tilde{A}_{22} \end{bmatrix}, \tilde{D} = \begin{bmatrix} 0 \\ \tilde{D}_2 \end{bmatrix}, \tilde{C} = [0 \quad I_p] \qquad (38)$$

Where $\tilde{A}_{11} = A_{11} + L\,A_{21}$ is stable and $\tilde{D}_2 = TD_2$
The reconstructed actuator fault is given by:

$$\hat{f}_{ac} \approx \tilde{D}_2{}^+ P_0^{-1}\ \vartheta_{\acute{e}q} \qquad (39)$$

Where $\vartheta_{\acute{e}q}$ is the equivalent DIS, which has the following structure:

$$\vartheta_{\acute{e}q} = -\alpha\|P_0\varepsilon_y\|.\|P_0\,\tilde{D}_2\|\frac{P_0\varepsilon_y}{\|P_0\varepsilon_y\| + \delta} \qquad (40)$$

α is chosen to be $2.5.10^4$, while δ represents a small positive numerical value.

In this paper, the matrix D is chosen to be equal to B.

3.5. Formulation of the actuator faults

Fault reconstruction holds crucial significance, particularly in wind energy, where it enhances operational reliability by identifying and addressing potential failures. Facilitating early detection of anomalies, it strengthens operational safety, minimizes disruptions, and optimizes system performance. Additionally, fault reconstruction contributes to reducing maintenance costs by intervening before issues lead to major failures. It also provides a better understanding of system operation in the presence of faults, guiding the development of more resilient and robust solutions. In summary, fault reconstruction plays a pivotal role in proactive maintenance, ensuring safety, and enhancing operational efficiency in critical contexts such as wind energy.

Five specific faults can affect pitch actuators: wear of the pump, leakage in the hydraulic system, high air content in the hydraulic oil, blockage in the valve, and blockage in the pump. Notably, valve blockage and pump blockage exhibit similar effects on the pitch system, leading to their classification as the same fault in many cases. On the other hand, hydraulic leakage, pump wear, and high air content in the hydraulic oil are considered faults that alter the dynamics of the pitch system, causing a deceleration in control actions and subsequently resulting in suboptimal power production. Consequently, these three faults are treated similarly in the analysis.

The modifications in the dynamics of the pitch system stem from the changes in parameters ξ_i and ω_n denoted in equation (2), where they take defective values ξ_f and ω_f. These altered values affect the matrices A and B in the state-space representation, in equation (8).

This paper specifically focuses on hydraulic leakage in the considered wind turbine model. Two scenarios are examined: an extreme fault and a moderate fault. The parameters associated with these scenarios are organized and presented in Table 1.

Table 1. Pitch parameters and fault indicators in hydraulic leakage faults

Fault scenario	$\omega\ (\frac{\text{rad}}{\text{s}})$	ξ_i	α_f
Fault-free	$\omega_n = 11{,}11$	$\xi = 0{,}6$	0
Extreme fault	$\omega_l = 3{,}42$	$\xi_l = 0{,}9$	1
Moderate fault	$\omega_f = 6{,}72$	$\xi_f = 0{,}2$	0.7

ω_n and ξ are the fault free parameters, ω_l and ξ_l are the limit parameters in hydraulic leakage that correspond to 50% of the nominal pressure, ω_f and ξ_f are the parameters faulty in hydraulic leakage. It can be written as:

$$\omega_f^2 = \omega_n^2 + \alpha_f(\omega_l^2 - \omega_n^2) \tag{41}$$

$$2\xi_f\omega_f = 2\xi\omega_n + \alpha_f(2\xi_l\omega_l - 2\xi\omega_n) \tag{42}$$

Where $\alpha_f \in [0,1]$ is the fault indicator for hydraulic leakage $\alpha_f = 0$ in free fault and $\alpha_f = 1$ if the pressure loses half of its nominal value, it is noted that $\dot{\alpha}_f(t) \geq 0$ for all t since a leak cannot be stopped without system repair.

The generator and converter system can have two types of faults: a shift in dynamics due to changes in the generator's specific parameter α_{gc}, or an offset in the converter's torque. These issues arise from internal complications, like faults in the converter's electronics or inaccuracies in torque estimation [5]. These problems can lead to serious consequences, notably a slower control of torque due to changes in dynamics. The offset fault, which leads to below-optimal wind turbine power output and develops quickly, is deemed a medium-severity issue. The previously stated faults that influence the actuation of the generator are modelled as:

$$\dot{\tau}_g = -\alpha_{gc}\,\tau_g + \alpha_{gc}\tau_{gref} + f_{\tau_g} \tag{43}$$

Where: f_{τ_g} represents the fault affecting the actuation of the generator and converter.

The matrices A_f and B_f in faulty condition are written as:

$$A_f = A + \Delta A \tag{44}$$
$$B_f = B + \Delta B \tag{45}$$

Where ΔA *and* ΔB represent the deviation from nominal operation due to the fault.

Define $h = \omega_l^2 - \omega_n^2$, $g = 2\xi_l\omega_l - 2\xi_n\omega_n$ and $f_{ac} = [f_1 \quad f_2 \quad f_3]^T$.

By employing equations (41), (42) and (43), along with the fact that D is equal to B in equation (10), and by establishing an identification between the relationships expressed in equations (44) and (45) on one side, and equation (10) on the other side, we can deduce the following:

$$f_1 = \frac{f_{\tau_g}}{\alpha_{gc}},\ f_2 = 0,\ \text{and}\ f_3 = \frac{\alpha_f}{\omega_n^2}\left(h\,\beta_r - g\,\dot{\beta}\right) \tag{46}$$

Therefore, the reconstruction of f_{ac} provides access to the fault signal f_{τ_g} and the fault indicator α_f.

3.6. Observer parameters

The primary energy source for the wind system is the aerodynamic torque, as indicated by equation (1), serving as the second input for equation (8). The wind turbine controller provides the first and third inputs. Detailed technical characteristics and numerical values of the parameters for the simulated wind turbine in this study can be found in Odgard et al. [5]. The suggested observer is based on the structure outlined in equation (13), with alterations made to the switching term indicated in equation (17). The process involves the application of an algorithm akin to the one elucidated in [22], the design parameters were set to be:

$$U_w = 0.6 I_6\ ,\ V_w = I_5,\ \text{and}\ \delta = 1e^{-3}$$

The matrices P_0 and $\widetilde{D}_2$ from (36) are given as:

$$P_0 = \begin{bmatrix} 0.0021 & 0.0010 & 0 & 0 & 0.0000 \\ 0.0010 & 1.4926 & 0 & 0 & 0.0000 \\ 0 & 0 & 0.7158 & 3.7298 & 0 \\ 0 & 0 & 3.7298 & 35.1656 & 0 \\ 0.0000 & 0.0000 & 0 & 0 & 122.6318 \end{bmatrix},$$

$$\widetilde{D}_2 = \begin{bmatrix} 0 & 0 & 0 \\ 0 & 0 & 0 \\ 0 & 1.81e^{-8} & 0 \\ 0 & 0 & 1.234e^{2} \\ 0 & 0 & 0 \\ 50 & 0 & 0 \end{bmatrix}$$

The associated gains from the observer representation in (13) are:

$$G_l = \begin{bmatrix} 488.7675 & 0.8309 & 0 & 0 & -0.0000 \\ 0.8309 & 0.6756 & 0 & 0 & 0.0000 \\ 1.0412 & 0.0055 & 0 & 0 & 0.0000 \\ 0 & 0 & 3.1233 & -0.3313 & 0 \\ 0 & 0 & -0.3313 & 0.0636 & 0 \\ -0.0000 & 0.0000 & 0 & 0 & 0.0082 \end{bmatrix},$$

$$G_n = \begin{bmatrix} 487.9009 & -0.3226 & 0 & 0 & -0.0000 \\ -0.3226 & 0.6702 & 0 & 0 & -0.0000 \\ 1.0347 & -0.0007 & 0 & 0 & -0.0000 \\ 0 & 0 & 3.1233 & -0.3313 & 0 \\ 0 & 0 & -0.3313 & 0.0636 & 0 \\ -0.0000 & -0.0000 & 0 & 0 & 0.0082 \end{bmatrix}$$

4. SIMULATION RESULTS

The objective of this study is to reconstruct actuator faults in the generator/converter and pitch system. Firstly, these faults are considered separately and then simultaneously. To test the effectiveness of our fault reconstruction approach, a signal representing the fault was injected at the system input, which was initially unknown to the system. The previously described method was then used to reconstruct the fault and evaluate the performance of the adopted reconstruction approach. The wind speed profile used in the simulation shown in Figure 2, which is highly variable, is based on real wind speed data sourced from a wind farm [5].

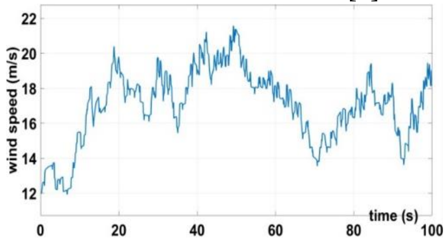

Fig. 2. The stochastic wind speed profile taken into account during the simulation

4.1. Faults separately

Two scenarios involving hydraulic leakage faults have been established for the hydraulic pitch actuator: an extreme fault and a moderate fault. The pitch subsystem parameters, along with the associated fault indicators, can be found in Table 1. The first of these fault scenarios encompasses a sudden decrease in hydraulic pressure caused by a leak within the hydraulic system. The corresponding actual fault indicator is $\alpha_f = 1$. This fault is considered from 20s to 45s, during which the parameters ω_n and ξ undergo a change in values, transitioning to ω_f and ξ_f, respectively. By employing the proposed SMO, the actuator fault $\hat{f}_{ac}$ is reconstructed. The fault indicator α_f and its estimated $\widehat{\alpha_f}$ are presented in Figure 3. This figure clearly demonstrates the prompt detection and precise reconstruction of the fault , the maximal relative gap is 0,5%. During the moderate fault scenario, the fault indicator α_f is assigned a value of 0.7 from 50 s to 70 s. The estimated fault indicator $\widehat{\alpha_f}$ is depicted in Figure 4. Notably, the estimated indicator closely aligns with the actual one, resulting in a reasonably precise estimation of the pitch actuator parameters and , the maximal relative gap is 0,7%.

The generator fault is also simulated. It runs from 75 s to 90 s. The fault is intermittent and introduces a consistent amplitude bias. The real generator fault f_{τ_g} and its estimated $\widehat{f_{\tau_g}}$ are illustrated in Figure 5. The acquired outcome demonstrates that the reconstructed fault closely and precisely mirrors the actual fault, the relative gap is: $3{,}3.10^{-3}\%$.

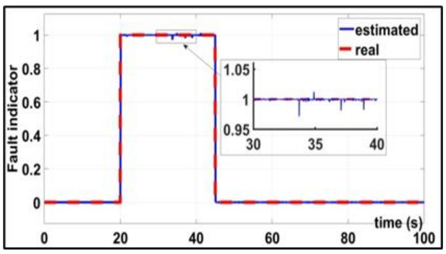

Fig. 3. Fault indicator $\boldsymbol{\alpha_f}$ and its corresponding estimation $\widehat{\boldsymbol{\alpha_f}}$ in the extreme fault case

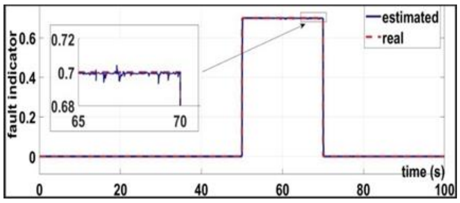

Fig. 4. Fault indicator α_f and its corresponding estimation $(\hat{\alpha}_f)$ in the moderate fault case

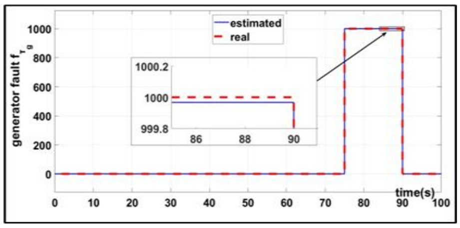

Fig. 5. Real generator fault f_{τ_g} and its estimated $(\hat{f}_{\tau_g})$

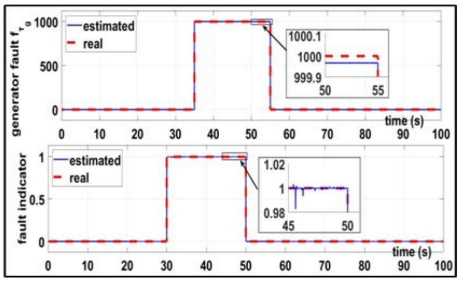

Fig. 6. Real and Estimated Simultaneous Faults: generator fault f_{τ_g} and its estimation $(\hat{f}_{\tau_g})$ (top), and fault indicator α_f and its estimation $(\hat{\alpha}_f)$ (bottom).

4.2. Faults simultaneously

In this case, both the leakage faults in the pitch system and the fault in the generator are simultaneously treated. Figure 6 illustrates this situation: the leakage fault is treated in an extreme fault condition between 30 s and 50 s, while the fault affecting the generator torque occurs between 35 s and 55 s. Consequently, these two faults happen concurrently within the [35s, 50s] timeframe. The maximum relative gap for the leakage fault is determined to be 1.7% , whereas for the generator fault, it is calculated to be $3{,}4.10^{-3}\%$. Hence, the simulation results confirm the precise identification and reconstruction of the faults. This supports the modification introduced to the SMO, as mentioned in paragraph 3.

5. CONCLUSION

In this study, a sliding mode observer enhanced with a modified DIS is presented to estimate the pitch actuator fault and generator torque actuator fault in wind turbine systems. Two scenarios are detailed. In the first, separate faults are assessed, with the hydraulic leakage fault simulated under both extreme and moderate conditions, followed by the generator actuator fault. In the second scenario, both the hydraulic leakage fault (under extreme conditions) and the generator torque actuator fault are simulated concurrently, using the same switching term of the SMO. Results indicate the accurate estimation of the hydraulic leakage fault using the introduced fault indicator and the precise reconstruction of the generator actuator fault. This underscores the efficacy of the modification made to the SMO's switching term.

Source of funding: *This research received no external funding.*

Author contributions: *research concept and design, M.T.; Collection and/or assembly of data, M.T.; Data analysis and interpretation, M.T.; Writing the article, M.T.; Critical revision of the article, A.E.O.; Final approval of the article, B.T.*

Declaration of competing interest: *The authors declare that they have no known competing financial interests or personal relationships that could have appeared to influence the work reported in this paper.*

REFERENCES

1. Letcher T. Wind energy engineering: a handbook for onshore and offshore wind turbines. Elsevier; 2023.
2. Zouirech S, Zerouali M, El Ougli A, Tidhaf B. Maximum Power Extraction from a Wind Turbine Energy Source Based on Fuzzy and Conventional Techniques for Integration in Micro-Grid. International Conference on Electronic Engineering and Renewable Energy 2020: 819-829. https://doi.org/10.1007/978-981-15-6259-4_86.
3. Mary SA. Fault Diagnosis and Control Techniques for Wind Energy Conversion System: A Systematic Review. Third International Conference on Intelligent Computing Instrumentation and Control Technologies (ICICICT) 2022: 700-704. https://doi.org/10.1109/ICICICT54557.2022.9917722.
4. Li J, Wang S. Dual multivariable model-free adaptive individual pitch control for load reduction in wind turbines with actuator faults. Renewable Energy 2021; 174: 293-304. https://doi.org/10.1016/j.renene.2021.04.080.
5. Odgard PF, Stoustrup J, Kinnaert M. Fault-Tolerant Control of Wind Turbines: A Benchmark Model. IEEE Transactions on Control Systems Technology 2013; 21: 1168–1182 https://doi.org/10.1109/TCST.2013.2259235.
6. Djoudi HCB, Hafaifa A, Djoudi D, Guemana M. Fault tolerant control of wind turbine via identified fuzzy models prototypes. Diagnostyka 2020; 21(3): 3-13. https://doi.org/10.29354/diag/123220.
7. Azzouzi M, Diarra R, Popescu D. (2018). Fault diagnosis of sensors, actuators and wind turbine system. Diagnostyka; 2018, 19(4): 3-10. https://doi.org/10.29354/diag/93846.
8. Lan J, Patton RJ. Robust integration of model-based fault estimation and fault-tolerant control. Berlin/Heidelberg, Germany: Springer 2021. https://doi.org/10.1007/978-3-030-58760-4.
9. Ashwini P, Archana T. Observer-based robust fault-tolerant control for wind energy system. International Journal of System Assurance Engineering and Management 2021; 1-8. https://doi.org/10.1155/2018/5628429.
10. Zhao S, Xia J, Deng R, Cheng P, Yang Q. Adaptive Observer-Based Resilient Control Strategy for Wind Turbines Against Time-Delay Attacks on Rotor Speed Sensor Measurement. IEEE Transactions on Sustainable Energy 2023, 14(3): 1807-1821. https://doi.org/10.1109/TSTE.2023.3248862.
11. Cho S, Gao Z, Moan T. Model-based fault detection, fault isolation and fault-tolerant control of a blade pitch system in floating wind turbines. Renewable energy 2018, 120, 306-321. https://doi.org/10.1016/j.renene.2017.12.102.
12. Teng J, Li C, Feng Y, Yang T, Zhou R, Sheng QZ. Adaptive observer based fault tolerant control for sensor and actuator faults in wind turbines. Sensors 2021, 21(24), 8170. https://doi.org/10.3390/s21248170.
13. Chen J, Patton RJ. Robust model-based fault diagnosis for dynamic systems. Springer Science & Business Media 2012.
14. Sedigh Ziyabari SH, Aliyari Shoorehdeli M, Karimirad M. Robust fault estimation of a blade pitch and drivetrain system in wind turbine model. Journal of Vibration and Control 2021, 27(3-4): 277-294. https://doi.org/10.1177/1077546320926274.
15. Shi F, Patton R. An active fault tolerant control approach to an offshore wind turbine model. Renewable Energy 2015; 75: 788-798. https://doi.org/10.1016/j.renene.2014.10.061.
16. Mousavi M, Rahnavard M, Haddad S. Observer based fault reconstruction schemes using terminal sliding modes. International Journal of Control 2020, 93(4): 881-888. https://doi.org/10.1080/00207179.2018.1487082.
17. Taouil M, El Ougli A, Tidhaf B, Zrouri H. Sensor fault reconstruction for wind turbine benchmark model using a modified sliding mode observer. International Journal of Electrical and Computer Engineering 2023, 13(5): 5066-5075 http://doi.org/10.11591/ijece.v13i5.pp5066-5075.
18. Sloth C, Esbensen T, Stoustrup J. Robust and fault-tolerant linear parameter-varying control of wind turbines. Mechatronics 2011; 21(4): 645-659. https://doi.org/10.1016/j.mechatronics.2011.02.001.
19. Edwards C, Spurgeon SK. On the development of discontinuous observers. International Journal of control 1994; 59(5): 1211-1229. https://doi.org/10.1080/00207179408923128.
20. Alwi H, Edwards C, Tan CP. Fault detection and fault-tolerant control using sliding modes. London: Springer; 2011.

Mohammed TAOUIL
Received his master's degree in Electronics and Communication Systems from the Faculty of Science, Oujda, in 2008. He is currently a PhD student in the Laboratory of Electronics and Embedded Systems (LES), Team of Embedded Systems, Renewable Energy, and Artificial Intelligence, at the National School of Applied Sciences, Mohammed First University, Oujda, Morocco. His research interests include wind and photovoltaic energy. He can be contacted at email: t123med@hotmail.fr.

Abdelghani EL OUGLI
Received his PhD degree in Automation, Signals, and Systems from the Faculty of Sciences at Dhar el-Mehraz, University of Sidi Mohamed Ben Abdellah, in 2009 for his thesis titled "Integration of Fuzzy Techniques in the Synthesis of Adaptive Controllers." He is currently a professor at Sidi Mohamed Ben Abdellah University, a researcher, and a member of the team of the Computer Science, Signal, Automation, and Cognitivism Laboratory (LISAC), Faculty of Science, Sidi Mohamed Ben Abdellah University, Fez, Morocco. He can be contacted at email: a.elougli@yahoo.fr

Belkassem TIDHAF
is currently a professor and the head of the Department of Information Technology and Communication Networks at the National School of Applied Sciences, Mohammed First University in Oujda, Morocco. He is a researcher and a member of the Team of Embedded Systems, Renewable Energy, and Artificial Intelligence at the National School of Applied Sciences, Mohammed First University, Oujda, Morocco. He can be contacted at email: tidhaf@yahoo.com.